Strategies for laser-induced fluorescence detection of nitric oxide in high-pressure flames. II. *A–X*(0,1) excitation

Wolfgang G. Bessler, Christof Schulz, Tonghun Lee, Jay B. Jeffries, and Ronald K. Hanson

A–X(0,1) excitation is a promising new approach for NO laser-induced fluorescence (LIF) diagnostics at elevated pressures and temperatures. We present what to our knowledge are the first detailed spectroscopic investigations within this excitation band using wavelength-resolved LIF measurements in premixed methane/air flames at pressures between 1 and 60 bar and a range of fuel/air ratios. Interference from O_2 LIF is a significant problem in lean flames for NO LIF measurements, and pressure broadening and quenching lead to increased interference with increased pressure. Three different excitation schemes are identified that maximize NO/O_2 LIF signal ratios, thereby minimizing the O_2 interference. The NO LIF signal strength, interference by hot molecular oxygen, and temperature dependence of the three schemes are investigated. © 2003 Optical Society of America

OCIS codes: 280.1740, 300.2530.

1. Introduction

Nitric oxide (NO) is an important species in the chemistry of atmospheric ozone where it participates in the production of ozone in the urban troposphere and the destruction of ozone in the stratosphere. The atmospheric NO_x budget is dominated by combustion effluent, and a large fraction of these emissions originate from automotive engines and gas turbines where the combustion chamber is at high pressure. Despite the use of catalytic NO converters, cleaner engine exhaust would reduce the NO_x load on the atmosphere. Laser-induced fluorescence (LIF) is an important tool[1–3] to help the combustion engineer understand NO formation in practical combustion systems[3–13] and thus develop new schemes to minimize NO effluent. The high operating pressure of these practical combustors requires strategies for quantitative NO LIF measurements at pressures exceeding 50 bar.

Different approaches for NO excitation have been previously suggested, including NO excitation in the $D–X$(0,1) band and in several $A–X$ vibrational bands. Interference LIF from overlapped O_2 transitions becomes a serious problem in high-pressure lean or nonpremixed flames. The literature does not give clear guidelines on which transitions are favorable in a given diagnostic situation. We have examined NO LIF excitation and detection strategies in premixed methane/air flames as a function of equivalence ratio and pressures between 1 and 60 bar. Wavelength-dispersed LIF spectra are recorded versus excitation wavelength to select optimum excitation features and fluorescence collection bandpass. Interference LIF is quantified for each of the strategies studied. This work is the second in a series of papers in which we compare transitions in the $A–X$ band and recommend the most appropriate excitation and detection strategies for high-pressure NO LIF.[14,15] The first paper investigated different strategies with NO $A–X$(0,0) excitation.[14] Here we examine excitation of using NO $A–X$(0,1) band transitions. We select three regions that appear to have the least O_2 interference and study them in detail to quantify the degree of interference LIF. The comparison between transitions of different vibrational states including the influence of broadband interference in lean and rich flames is underway.[15]

2. Background

LIF measurements of NO in high-pressure combustion environments encounter a number of spectroscopic difficulties concerning signal strength and interference. These problems have been discussed in detail in our previous research,[14,16,17] and we will give just a short overview here.

- *Transmission properties.* UV light at short wavelengths (<250 nm) is absorbed by hot CO_2 and H_2O present in the combustion gases,[18] and absorption cross sections increase with temperature and decrease with wavelength.[19] The effect increases with pressure because of the increasing number density of absorbers, leading to strong attenuation of both laser and signal light even in small flame geometries.[20,21]
- *O_2 LIF interference.* Hot O_2 is the main contributor to LIF interference in lean and nonpremixed flames. The $B^3\Sigma^- - X^3\Sigma^+$ Schumann–Runge bands of O_2 overlap with the $A^2\Sigma^+ - X^2\Pi$ NO gamma bands over a wide range of excitation wavelengths[22] resulting in overlapping absorption features and fluorescence signals. O_2 LIF background increases with pressure for two reasons: variation in fluorescence quantum yield and variation in spectral overlap with the laser profile that results from line broadening.[23–25]
- *Interference in rich flames.* In rich and nonpremixed flames additional broadband fluorescence interference has been observed, which is usually attributed to polycyclic aromatic hydrocarbons and partially burned hydrocarbons (aldehydes, ketones).[9] In sooting flames at high laser energies, interference by LIF of laser-generated C_2 has also been reported.[26]

A large number of NO LIF measurements have been performed in high-pressure flames using $A–X(0,0)$ excitation at 224–227 nm.[4–7,20] This wavelength region, however, is severely affected by laser attenuation in high-temperature, high-pressure environments.[27,21] Attenuation can be significantly reduced by use of longer wavelengths that probe vibrationally excited states of the NO molecule. $A–X(0,2)$ excitation at 244–247 nm has found broad application thanks to the availability of strong excimer lasers providing appropriate excitation wavelengths.[8,9,27,28] However, the drawback of this approach is reduced signal strength caused by the small population of the $X (v'' = 2)$ state even at flame temperatures.

NO $A–X(0,1)$ excitation is not among the established NO excitation schemes frequently found in the literature for NO LIF measurements in flames or flows. Its application, however, is promising because it reduces laser beam attenuation [which is a problem with (0,0) excitation] while still providing strong signals [which is a problem with (0,2) excitation[16]]. Furthermore, the availability of optical parametric oscillator systems that provide high laser-pulse energies throughout the UV (up to 30 mJ) allows the application of (0,1)-excitation in the 233–237-nm wavelength region. To our knowledge, the first application of NO(0,1) LIF in high-pressure combustion was performed by Jamette *et al.*[29] in a direct-injection spark-ignition gasoline engine.

Laser beam attenuation also motivated Chou *et al.* to use $A–X(0,1)$ for LIF measurements in an atmospheric-pressure NH_3/O_2 flame to avoid quasi-continuum NH_3 absorption near 226 nm.[30] A similar strategy was chosen for LIF measurements[31] and cavity ring-down investigations[32] in closed-chamber low-pressure burners where cold NO from the exhaust gases can recirculate outside the flame and cause significant absorption of the laser beam. This absorption can be reduced with a (0,1) approach, since the $X (v'' = 1)$ state is populated mainly at hot flame temperatures, resulting in a low concentration of absorbing NO molecules in the cold recirculation gases.

Although the choice of excitation in different vibrational bands addresses the (broadband) transmission problem, the choice of a particular rotational absorption feature within the vibrational band is largely responsible for the contribution of (narrowband) O_2 LIF interference. Jamette *et al.*[29] chose the $R_1 + Q_{21}(22.5)$, $Q_1 + P_{21}(8.5)$, $Q_2 + R_{12}(17.5)$ feature at 236.22 nm on the basis of simulations of LIF excitation spectra of NO and O_2 in order to maximize the NO/O_2 LIF ratio. However, no experimental spectroscopic data were available to support this choice.

In the present study we compare different NO $A–X(0,1)$ excitation strategies in spectrally resolved LIF measurements in premixed methane/air flames with different air/fuel ratios. Excitation scans at 10 and 60 bar covering a broad spectral range are performed to search for possible transition "candidate" lines with minimum O_2 LIF interference. Three candidate transitions (including the choice of Jamette *et al.*[29]) are investigated in detail in lean and rich flames in the 1–60-bar range. In addition, we compare signal strength and temperature dependence.

3. Experiment

Laminar, premixed methane/air flat flames at pressures from 1 to 60 bar were stabilized on a porous, sintered stainless-steel plate of 8-mm diameter; this burner was mounted in a stainless-steel housing with an inner diameter of 60 mm with a pressure stabilization of ± 0.1 bar.[14,33] Investigations were performed for fuel/air equivalence ratios of $\phi = 0.83$, 0.93, 1.03, and 1.13. These equivalence ratios were chosen to allow direct comparison to earlier measurements at these flame conditions.[14] Unless otherwise stated, all measurements were carried out with 300-ppm (parts in 10^6) NO seeded to the feedstock gases to mimic enginelike conditions. Optical access to the flame was possible by means of four quartz windows (Fig. 1).

Laser light (1 mJ @ 233–238 nm, 0.4 cm^{-1} FWHM) from a Nd:YAG-pumped (Quanta Ray GCR250) frequency-doubled (β-barium borate) dye laser (LAS, LDL205, Coumarin 102) was aligned parallel to the burner surface and passed through the center of the
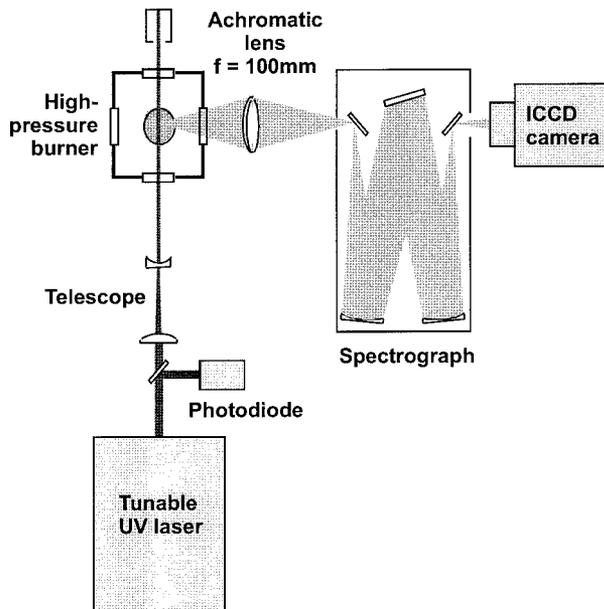
Fig. 1. Experimental arrangement.

Fig. 2. O_2 and NO LIF excitation spectra at 10 and 60 bar over a long spectral range within the NO $A–X(0,1)$ band. Candidate transitions with maximum NO/O_2 signal ratio are marked. 10 bar: NO LIF and O_2 LIF measured in a $\phi = 0.9$ methane/air, 400 ppm NO-doped flame. 60 bar: measured O_2 LIF in a flame without NO doping and simulated NO LIF for a similar flame. The NO and O_2 LIF intensities from both panels are comparable on a relative scale.

flame 2 mm above the burner matrix. The pulse energy was measured with a fast photodiode (LaVision). The beam was focused with a spherical lens to a diameter of 1.5 mm at the point of measurement. Fluorescence signals were collected at right angles to the laser beam and focused with a $f = 105$ mm, $f_\# = 4.5$ achromatic UV lens (Nikon) onto the horizontal entrance slit of a 250-mm imaging spectrometer (Chromex 250IS) equipped with a 600-groove/mm grating.

The dispersed fluorescence signals were detected with an intensified CCD camera (LaVision Flame-Star III). Each laser pulse yielded a complete fluorescence spectrum maintaining one-dimensional spatial resolution along the laser light path. The laser was tuned to record excitation spectra within the NO $A–X(0,1)$ band between 233 and 237 nm. The signal was averaged over 30 laser pulses for each excitation wavelength and stored for further evaluation before the laser was scanned to the next wavelength. The 30-shot averaged spectra were corrected for variations in laser-pulse energy.

The camera initially detects images with the spatial resolution along the horizontal path of the laser beam through the flame on one axis and spectral resolution showing emission spectra on the second axis. In these images the central area of the flame where temperature and concentrations are homogeneous is then chosen and integrated over the spatial axis, yielding a fluorescence spectrum. These spectra are stored in two-dimensional excitation-emission charts that contain the full spectral information and allow later evaluation of excitation as well as emission spectra with an arbitrarily selected bandpass. A more detailed explanation of this technique is given in Ref. 14.
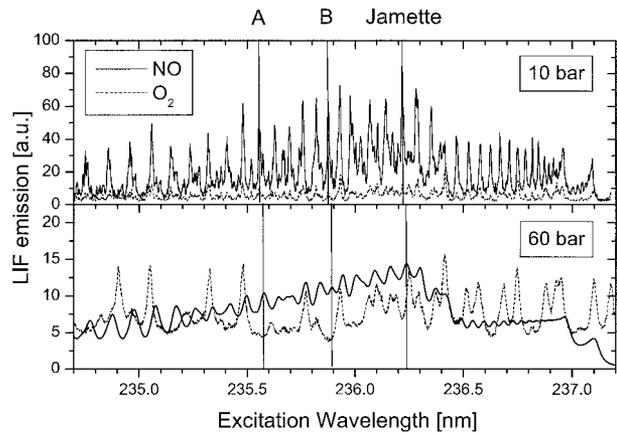
4. Results and Discussion

A. Choice of Candidate Transitions

Our objective in this study is to find transitions within the NO $A–X(0,1)$ band with minimum O_2 LIF interference and maximum signal strength. To identify possible transitions, excitation-emission charts were acquired at 1–60 bar in a $\phi = 0.9$ flame in the spectral range of 234.7–237.2 nm in 0.001-nm increments. This covers the part of the (0,1) band with the strongest transitions. Results are shown in Fig. 2. Whereas the 10-bar measurements were acquired with 400-ppm NO doping to the flame, the 60-bar measurements were performed without NO doping. For complete separation of NO and O_2 LIF 10-bar spectra, different emission bandpasses were selected for this illustration [220–230 nm for NO $A–X(0,0)$ emission and 251–255 nm for O_2 $B–X$ emission]. The quantitative comparisons later in this paper, however, use the same bandpass for assessing the NO and O_2 LIF signal strength, and constant NO doping for all pressures.

With increasing pressure the O_2 LIF intensity dominates the overall signal in the observed spectral range. Measuring NO excitation spectra (without any contribution from the O_2 LIF signal) is not feasible in these flames without added NO. To illustrate the relative change of O_2 and NO spectra, in Fig. 2 we compare the measured O_2 LIF spectra with simulated NO spectra at 60 bar. This simulation is scaled to the experimental 10-bar NO LIF signal corrected for pressure-dependent excitation and fluorescence efficiency. Because of line broadening at 10 bar, each NO LIF peak corresponds to up to eight overlapping rotational lines. At 60 bar the NO spectra show a small amplitude variation (~0.1 nm

Table 1. Investigated Transitions in the NO *A–X*(0,1) Band

Candidate	Transition	Excitation Wavelength (nm)	Ground-State Energy ϵ/k (K)
A	$R_1 + Q_{21}(16.5)$, $P_2 + Q_{12}(32.5)$, $P_{21}(22.5)$, $O_{12}(40.5)$	235.55	3384–6950
B	$P_1(25.5)$, $R_1 + Q_{21}(11.5)$, $Q_1 + P_{21}(17.5)$	235.87	3040–4305
Jamette[29]	$R_1 + Q_{21}(22.5)$, $Q_1 + P_{21}(8.5)$, $Q_2 + R_{12}(17.5)$	236.22	2718–3660

broad) from groups of rotational lines on top of a broad NO LIF baseline.

At both pressures, strongest NO signals occur with excitation between approximately 235.5 and 236.5 nm. Investigating the 60-bar spectra in this region, we find that the two excitation wavelengths with minimum O_2 signals (near 235.6 and 235.9 nm) are coincident with local NO signal maxima. These positions are marked "A" and "B" in Fig. 2. The excitation-wavelength regions with maximum NO signal (236.25 nm) is almost coincident with a local O_2 minimum. This transition was used by Jamette *et al.*[29] and is marked "Jamette" in Fig. 2. These three candidate wavelength positions corresponding to maximum NO/O_2 signal ratios are chosen for further investigation. Their spectroscopic data are summarized in Table 1.

B. Excitation-Emission Charts around the Candidate Transitions

Short excitation scans in the wavelength regions of the three candidate transitions were performed. The scans allow the detailed investigation of line broadening and line shift and the assessment of fluorescence signal strengths. Excitation-emission charts are shown in Fig. 3 for all investigated pressures from 1–60 bar and equivalence ratios from 0.83–1.13. In this and all the following figures, the feedstock gases are seeded with 300-ppm NO.

The excitation wavelength scales individually for each of the charts shown. Since spectral features of NO become increasingly broad with pressure and at the same time transitions shift to longer wavelengths, the spectral resolution of the excitation wavelength
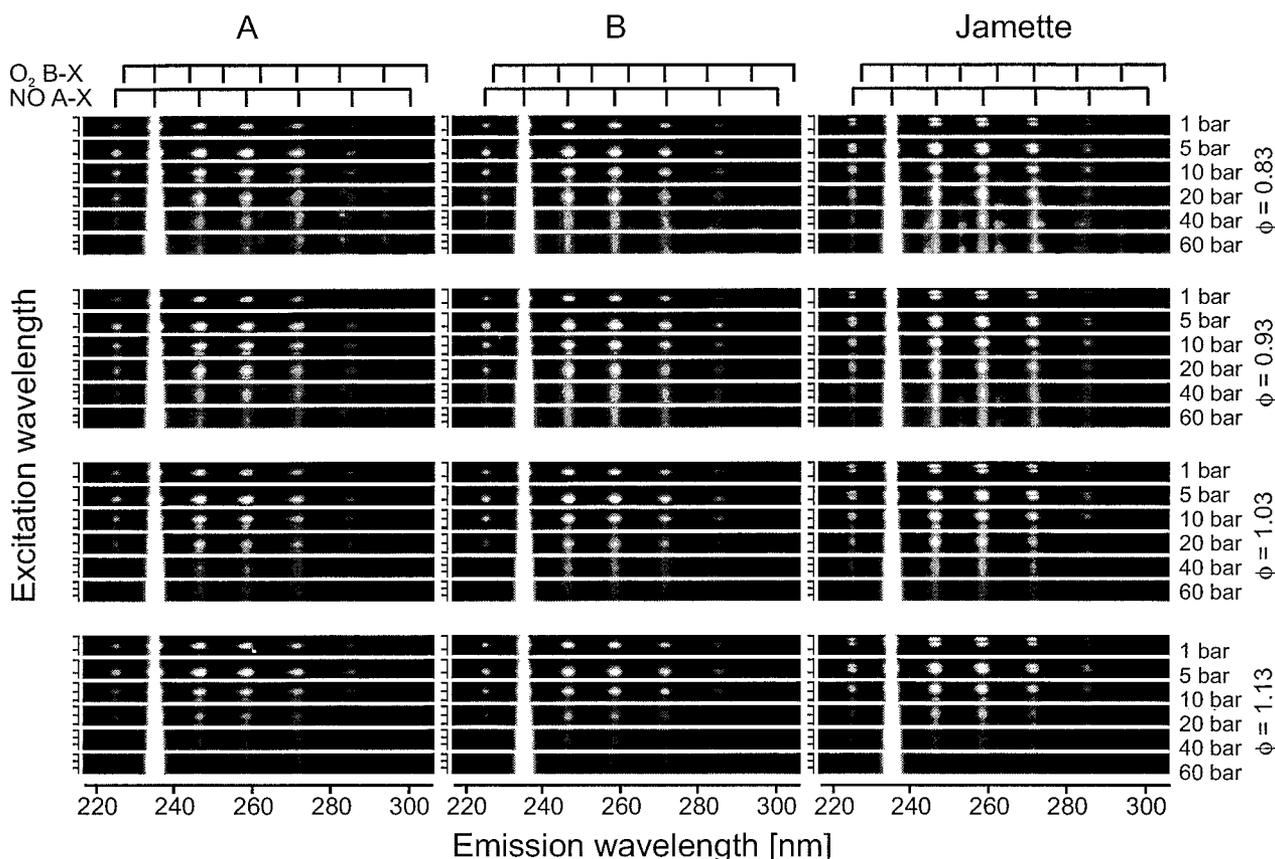

Fig. 3. Excitation-emission charts for excitation wavelengths around the three candidate transitions for all investigated pressures and equivalence ratios. The LIF signal intensity is gray-scale coded, and all values above an arbitrary threshold (corresponding to the NO (0,2) emission of the Jamette candidate at $p = 40$ bar, $\phi = 0.83$) are colored white. Excitation wavelength increases from top to bottom starting at 235.539, 235.859 and 236.209 nm for all A, B, and Jamette panels, respectively, and covering a range of 0.03, 0.045, and 0.06 nm for all 1 + 5, 10 + 20, and 40 + 60 bar panels, respectively. Intense Rayleigh scattering dominates NO and O_2 signals at 236 nm.

was reduced and the spectral range was increased with increasing pressure. For any of the three candidates, all charts start with the same lower excitation wavelength at their top (235.539, 235.859, and 236.209 nm for the A, B, and Jamette candidates, respectively), with increasing wavelengths per line from top to bottom in 0.001-nm steps for 1 and 5 bar, 0.0015-nm steps for 10 and 20 bar, and 0.002-nm steps for 40 and 60 bar; 30 lines are displayed in each chart.

The charts show major trends in signal strength and interference in a qualitative way. On the emission (x) axis, we find a strong signal from Rayleigh scattering around 235 nm. The vibrational progressions of the NO A–X and the O_2 B–X emissions can clearly be seen and distinguished; they occur both blue shifted and red shifted from the excitation wavelength. NO emission gets weaker with increasing pressure (owing to the variation in excitation efficiency, whereas the effects of fluorescence quantum yield and NO number density cancel) and, at high pressures, weaker with increasing equivalence ratio (owing to a decrease in NO concentration caused by reburn reactions that are known to be more efficient in rich flames[34]). O_2 emission gets stronger with increasing pressure (which is an effect of fluorescence quantum yield and number density; O_2 is excited to predissociative states) and weaker with increasing equivalence ratio (owing to a decrease in O_2 equilibrium concentration in the burnt gases). These effects are discussed in more detail in our previous paper.[14] They will be evident in the following subsections where we extract excitation and emission spectra from the charts of Fig. 2 for further evaluation.

C. Excitation Spectra

Fluorescence excitation spectra are shown in Fig. 4. The signal of the NO A–X(0,3) emission (257 nm) is plotted versus excitation wavelength for the $\phi = 0.93$ flames. The contribution of O_2 LIF to the emission is small in this fluorescence bandpass and will be further quantified in Subsection 4.E.

Collisional line broadening and line shifting has been investigated in detail for the NO molecule.[23–25] Its effect can be clearly seen in Fig. 4, as the signal peaks shift with pressure to longer excitation wavelengths. At the same time, line broadening becomes significant, leading to a loss in rotational structure for pressures of ≥ 10 bar, which is especially evident for the double peak of the Jamette transition feature. For all investigated transitions, the peak signal strength increases slightly between 1 and 5 bar and then decreases again for increasing pressure as discussed in Subsection 4.B.

An optimized strategy for NO detection should involve excitation at a wavelength yielding maximum signal strength for each individual pressure. From Fig. 4 it is evident that this can be achieved only by means of tuning the laser by several wave numbers as the pressure increases from 1 to 60 bar. In practical applications, however, pressure often varies rapidly (e.g., in internal combustion en-
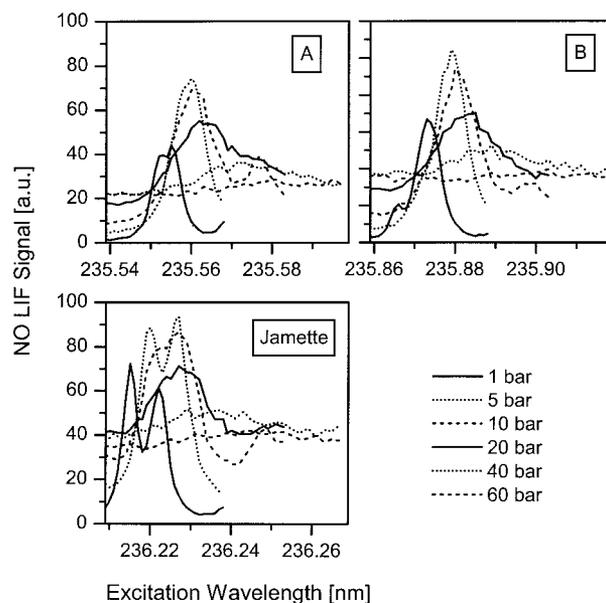

Fig. 4. Fluorescence excitation spectra for the three candidate transitions for the lean, $\phi = 0.93$ flames. The NO LIF signal is measured in the A–X(0,3) emission band around 258 nm.

gines). Here a fixed excitation wavelength must be chosen. The resulting signal loss is most pronounced for pressures between 1 and 5 bar because of the simultaneous action of pressure broadening and pressure shift. Interestingly, this effect is strongly reduced when we use the Jamette transition with its double peak. A laser wavelength of 236.22 nm (see Table 1) corresponds to the higher-wavelength peak at 1 bar. At 10 bar the transition has shifted by a wavelength increment that corresponds approximately to the splitting of the double peak, resulting in an overall increase in signal at this fixed wavelength between 1 and 10 bar. The other candidates, however, show a constant or even decreasing signal strength between 1 and 10 bar if the laser wavelength is held fixed at the 1-bar peak position.

The variation of signal strength with pressure can be described with use of collisional broadening and shifting models.[14] Therefore the effect can be corrected in practical applications with known or separately measured pressure even if total signal is reduced as a consequence of nonoptimized excitation.

D. Emission Spectra

Fluorescence emission spectra are extracted as horizontal profiles from the two-dimensional excitation-emission charts shown in Fig. 2. An arbitrary excitation wavelength can be chosen from the charts. Following the discussion in Subsection 4.C, we apply two strategies for this choice:

(1) constant excitation wavelength for all pressures corresponding to the excitation peak at 1 bar (often used in practical applications) and
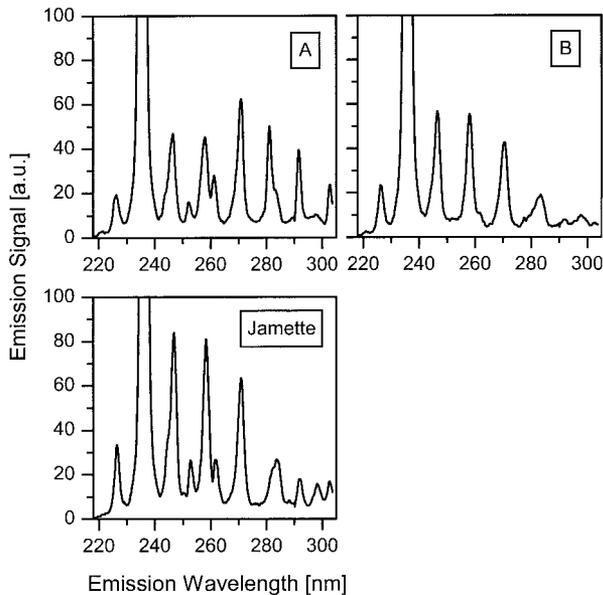
Fig. 5. Fluorescence emission spectra for the three candidate transitions for the $p = 40$ bar, $\phi = 0.83$ flame. At ~235 nm intense Rayleigh scattering adds to the NO (0,1) LIF signal.
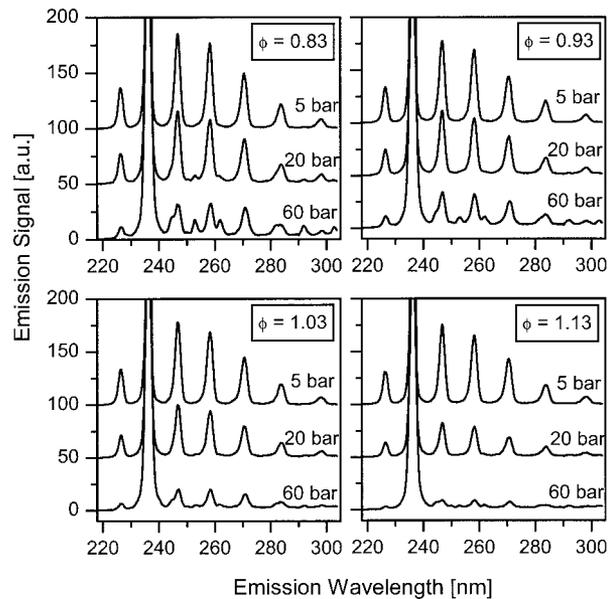

Fig. 6. Fluorescence emission spectra for the Jamette transition for the $p = 5$, 20 and 60 bar, $\phi = 0.83$, 0.93, 1.03, and 1.13 flames. At ~235 nm intense Rayleigh scattering adds to the NO (0,1) LIF signal.

(2) individual excitation wavelength for each pressure corresponding to maximum NO/O_2 LIF ratio.

The latter strategy involves a shift of excitation position to longer wavelengths with increasing pressure, following the shift of the transition peak, except when this would result in a stronger O_2 emission (which is the case for the Jamette transition where strong O_2 absorption features are present close to the 1-bar NO peak position).

In this subsection we only show a limited number of emission spectra corresponding to strategy (1) to demonstrate their typical behavior. Further data reduction leads to the more compact information presented in the following sections. Figure 5 shows emission spectra for the $p = 40$ bar, $\phi = 0.83$ flames for the three candidate transitions. Again, as in Fig. 2, the Rayleigh signal around 235 nm is dominant, and O_2 and NO LIF vibrational progression can easily be distinguished. The relative intensities of the NO emission peaks reflect the Franck Condon coefficients,[35] convoluted with the collection and detection efficiency of the spectrograph and camera system, which has a maximum at approximately 280 nm. The difference in NO/O_2 ratios can be seen in a qualitative way for the three candidates. For all three candidates a broadband background signal is evident, red shifted from the excitation wavelength. This background is further discussed in Subsection 4.F.

The influences of pressure and equivalence ratio on the NO and O_2 LIF emissions are shown in Fig. 6 for the Jamette transition. Emission spectra are shown for $p = 5$, 20, and 60 bar and equivalence ratios of 0.83, 0.93, 1.03, and 1.13. The relative O_2 interfer-

ence increases with increasing pressure and decreasing equivalence ratio.

E. NO Signal Strength and O_2 LIF Interference

For further discussion of the signal strengths the contributions of NO and O_2 LIF to the emission spectra were evaluated with a nonlinear least-squares fitting procedure to separate the overlapping signals. Because of the intense Rayleigh signal, the Voigt-type spectrograph slit function, and the presence of a broadband background signal, the multiple Gaussian fit that was applied in our earlier study[14] was not successful here. Instead, the intensities of simulated NO and O_2 LIF emission spectra, a Rayleigh signal, and a broadband background signal (see Subsection 4.F) were simultaneously fitted to the experimental data. The O_2 LIF emission spectra are complex because of overlapping absorption lines that lead to simultaneous excitation into multiple vibrational states. Furthermore, vibrational energy transfer in the upper electronic (B) state was evident from the O_2 LIF emission structure. Therefore emission signals from multiple upper vibrational states were fitted independently. Prior to the fit the experimental data were corrected for the wavelength-dependent detection efficiency and signal absorption from hot exhaust gases.[19,21] The overall fit was able to reproduce the experimental data well. An example is shown in Fig. 7 for the B candidate transition.

In practical applications planar LIF experiments are usually performed; the two-dimensional collection restricts the detection bandwidth to selection with bandpass filters. For excitation of NO in the $A-X(0,1)$ band such a detection is possible blue-shifted [$A-X(0,0)$ emission near 226 nm] or red-
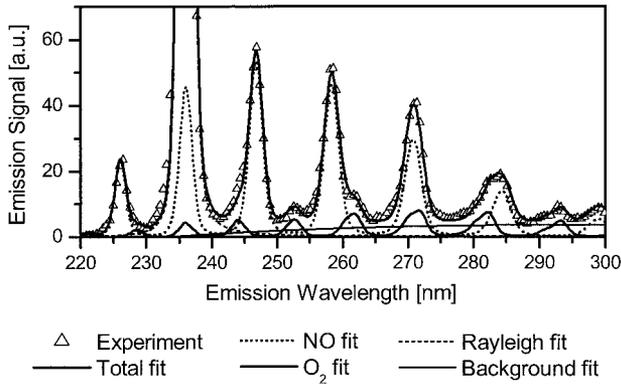
Fig. 7. Example of the nonlinear least-squares fit of simulated NO, O_2, and Rayleigh emission spectra (represented as Voigt line shapes) and a broadband background signal for the B candidate line at $p = 60$ bar, $\phi = 0.83$. See text for details.

shifted [$A–X(0,2)$, $(0,3)$, $(0,4)$, . . . emissions near 247, 259, and 272 nm, respectively] relative to the excitation wavelength (near 235 nm).

Total NO LIF signals between 220 and 230 nm [corresponding to blue-shifted detection of the $(0,0)$ emission] versus pressure are shown in Figs. 8 and 9 for excitation strategy (1) (constant excitation wavelength) and (2) (variable excitation wavelength), respectively. For strategy (1) (Fig. 8), the Jamette transition clearly yields largest NO LIF signals for all investigated flames, whereas the A and the B transitions show similar, reduced signals. The difference is large mainly at intermediate pressures (5–20 bar) where Jamette excitation leads to as much as 2.5 times stronger signals. This is due to the effect of the double peak of this transition (see Subsection
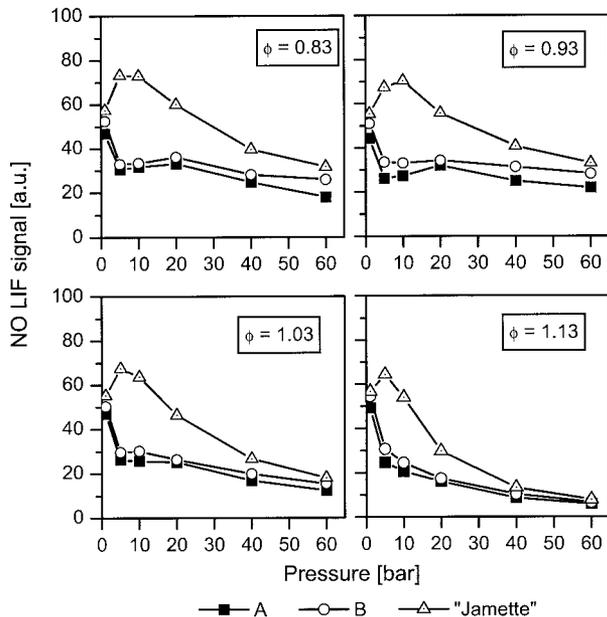

Fig. 8. Total NO fluorescence signal between 220 and 230 nm for the candidate transitions. The excitation wavelength is held constant with pressure corresponding to the NO signal peak at 1 bar. The scale is comparable for all panels of Figs. 8 and 9.
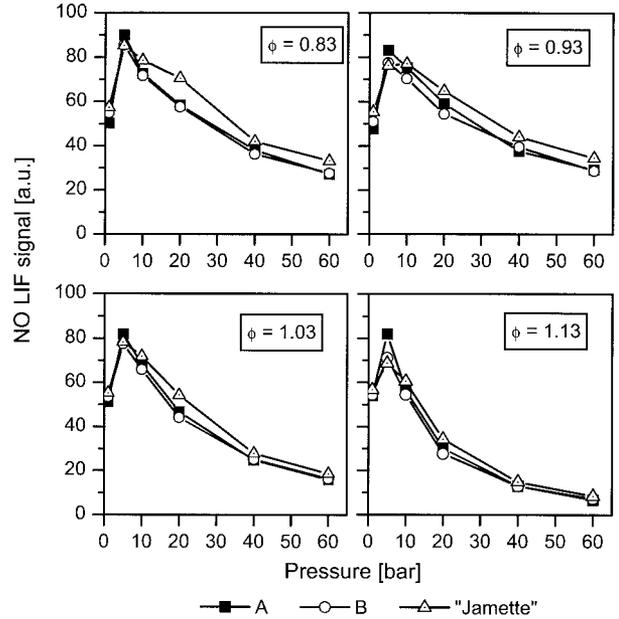

Fig. 9. Total NO fluorescence signal between 220 and 230 nm for the candidate transitions. The excitation wavelength is chosen for maximum NO/O_2 signal ratio for each individual pressure. The scale is comparable for all panels of Figs. 8 and 9.

4.C). For strategy (2) with optimized excitation (Fig. 9) signals are generally stronger, especially for $5 < p < 40$ bar, and the differences between the three candidates are only minor ($<15\%$). Again, the Jamette transition is slightly superior to the others.

For red-shifted detection of the $(0,2)$ and $(0,3)$ bands, NO signal intensities show the same relative behavior for the different candidates, but signals are generally stronger because of the combined effects of larger Franck–Condon factors, higher detection efficiency of the camera system, and (at high pressures) reduced signal absorption by hot exhaust gases. Furthermore, by using appropriate filters, integration over multiple emissions is easily achieved. From the Franck–Condon factors, integrated detection of the $(0,2)$ and $(0,3)$ bands (240–265 nm) leads to an increased signal of 83% in comparison with the $(0,0)$ band (220–230 nm).

For NO detection in lean flames not only a large signal strength but also a minimum O_2 LIF interference is desired. The fraction of O_2 interference in the total NO and O_2 LIF signal is quantified in Figs. 10 and 11 for excitation strategies (1) and (2), respectively. In both figures the results are shown for blue-shifted detection between 220 and 230 nm [corresponding to the NO $(0,0)$ emission] and for red-shifted detection between 240 and 265 nm [corresponding to the NO $(0,2)$ and $(0,3)$ emission] in the upper and lower parts of the figures, respectively. Only results for the lean flames are shown, since O_2 signal is low in the rich flames and since NO number density is strongly decreasing in rich flames at higher pressures as a result of reburn reactions. In the lean flames the NO concentration present at the point of measurement is approximately 300 ppm for all
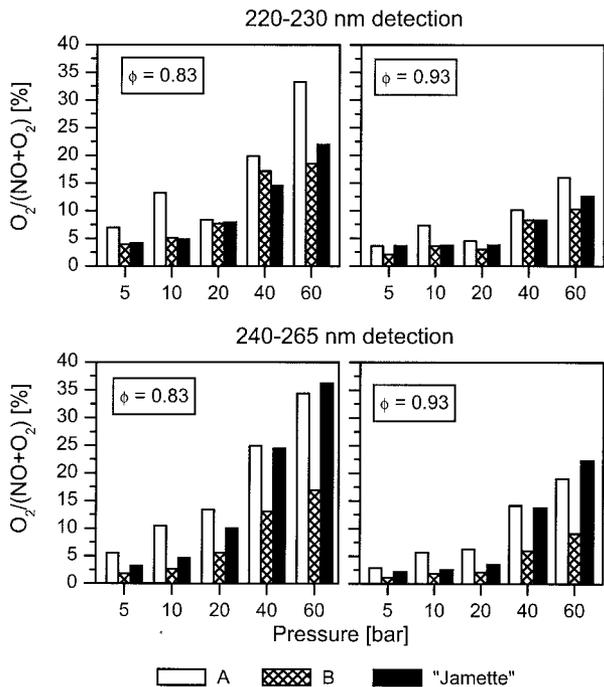
220-230 nm detection

240-265 nm detection

A   B   "Jamette"

Fig. 10. O_2 LIF contribution to the total NO + O_2 LIF signal for blue- and red-shifted detection.   The excitation wavelength is held constant with pressure corresponding to the NO signal peak at 1 bar.

pressures, corresponding to the natural NO present in the flame plus the amount seeded (300 ppm), reduced by reburn reactions ($\sim$10%).[20] At atmospheric pressure, no O_2 LIF signal could be detected for any of the candidate transitions.

220-230 nm detection

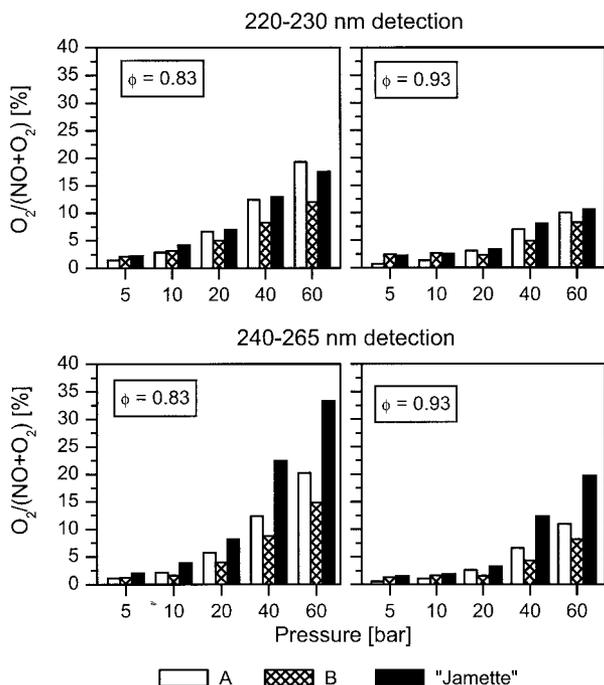**240-265 nm detection**

A   B   "Jamette"

Fig. 11. O_2 LIF contribution to the total NO + O_2 LIF signal for blue- and red-shifted detection.   The excitation wavelength is chosen for maximum NO/O_2 signal ratio for each individual pressure.

For excitation strategy (1) (Fig. 10) with blue-shifted detection a high O_2 LIF interference (33% for p = 60 bar, ϕ = 0.83) is present for the A excitation strategy, whereas the B and the Jamette transitions show less interference (maximum of $\sim$20%) at all pressures.   With red-shifted detection the B transition shows similar O_2 LIF interference (18% for p = 60 bar, ϕ = 0.83) but is clearly advantageous to the other candidates, which show a much larger O_2 interference of up to 36%.   It should be noted that the B transition shows least interference despite the low NO signal strength compared with the Jamette transition (Fig. 8).

For the optimized excitation strategy (2) (Fig. 11) O_2 LIF interference is generally lower.   There are nevertheless distinct differences for the three candidates.   The B candidate shows least interference in all cases (12% and 15% at p = 60 bar, ϕ = 0.83 for blue- and red-shifted detection, respectively).   The Jamette candidate leads to high interference especially with red-shifted detection ($\sim$33% for p = 60 bar, ϕ = 0.83).   The performance of the A candidate is intermediate.

The different excitation and detection strategies can be summarized as follows:

1.   In rich flames where O_2 LIF interference is not important, Jamette excitation yields maximum signal strength, especially when the laser is kept at a fixed wavelength.

2.   In lean flames where O_2 LIF interference is important, the best scheme for minimizing the interference is B excitation for fixed as well as varying laser wavelength.

3.   Tuning the laser wavelength to an optimized value to follow the pressure shift of the NO absorption feature is generally advantageous.

4.   Red-shifted detection is advantageous in terms of signal strength for all strategies. O_2 LIF interference is approximately equal for red- and blue-shifted detection for the A and the B candidates.   For Jamette excitation, red-shifted detection yields almost a factor of 2 higher O_2 LIF interference than blue-shifted detection despite higher signal strengths.

LIF interference can be further reduced by selection of narrower detection bandpasses, e.g., 240–250 nm instead of 240–265 nm, with, however, reduced total NO signal intensity.

F.   Broadband LIF Background

The emission spectra in Figs. 5 and 7 show a broadband background signal that is present mainly at long emission wavelengths.   This characteristic background was found for excitation throughout the investigated excitation wavelength range within the NO $A–X$(0,1) band independent of NO or O_2 resonances, increasing with pressure, and relatively independent of the equivalence ratio.   We assessed this background in the fitting procedure.   The spectral shape was determined from a 60-bar ϕ = 1.13 flame with the laser tuned away from the NO reso-
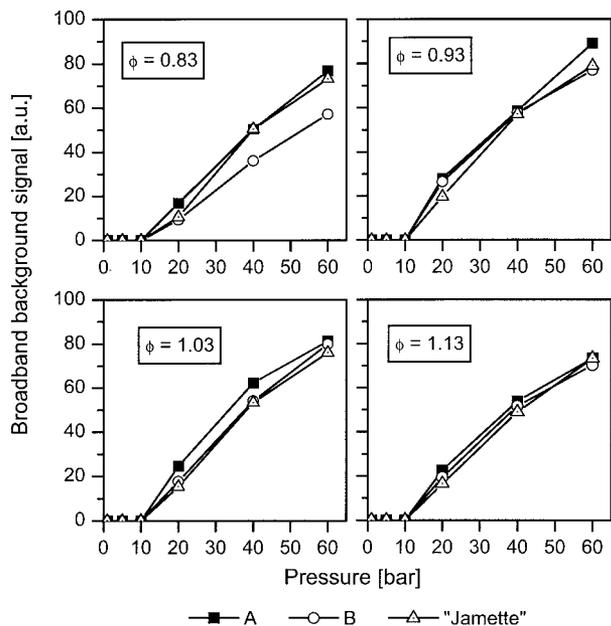
Fig. 12. Broadband background signal. The scales for the different air/fuel ratios are identical.

Fig. 13. Ratio of NO LIF emission of ~300 ppm NO in the flame gases (for details see text) over total emission in the 240–265-nm detection bandpass. The excitation wavelength is chosen for maximum NO/O_2 signal ratio for each individual pressure.

nance maximum (providing least NO and O_2 signals). Broadband emission was found only red shifted from the excitation wavelength. The spectral shape was kept in the fit for all flame conditions, and only the intensity was varied.

Figure 12 shows the intensity of the background signal for the investigated flames. The signal is approximately constant for excitation at all three candidate wavelengths (we believe that the scatter at high pressures in the $\phi = 0.83$ flames is due to fitting errors induced from the relatively strong O_2 signals), and it rises approximately linearly with pressure. The signal is only weakly dependent on equivalence ratio, with a slight increase from $\phi = 0.83$ to 0.93 followed by a decrease of ~25% to $\phi = 1.13$. This behavior is similar for all pressures.

The background signal contributes significantly to the total red-shifted emission. We quantified the ratio of the NO LIF signal to the total emission (O_2 LIF + NO LIF + background) for a 240–265-nm bandpass. This ratio is a measure for the purity of the detected signal. Despite the constant NO seeding (300 ppm in the fresh gases), actual NO concentrations decrease in rich flames on account of reburn reactions. The NO LIF/background ratio is therefore biased. To enable a comparison of the purity, we use the NO LIF signal strength measured in the $\phi = 0.93$ flame and compare it with the background signal observed in the $\phi \geq 1$ flames. Because the variation of fluorescence quantum yield is $\leq 6\%$ for these equivalence ratios[20] and the temperature sensitivity of the LIF signal is weak (see Subsection 4.G), this represents the expected NO LIF signal intensity of ~300 ppm NO and therefore enables the estimate of the purity in rich flames.
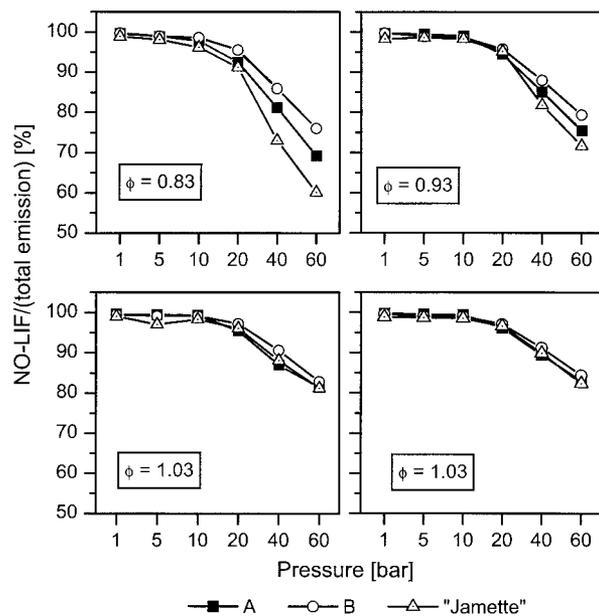
The resulting ratios NO LIF/(total emission) for

the optimized excitation strategy (individual excitation wavelengths for each pressure) are plotted in Fig. 13. In the lean flames, both O_2 LIF and the background cause a decrease in NO LIF purity to 60% at 60 bar for the Jamette candidate. The differences between the candidates are caused by the varying O_2 LIF signal strengths in the lean flames. However, even for rich flames where only the broadband emission is the dominant background, the purity is as low as 82% for the 60-bar flames and is similar for the three candidates.

The origin of this background is not yet known. Since its intensity is only slightly dependent on equivalence ratio, it is unlikely that it is LIF from polycyclic aromatic hydrocarbons that are present mainly in rich flames. Since hot CO_2 and H_2O combustion products show broadband UV absorption,[19,21] a possible interpretation for the background might be fluorescence from these species. In this case the variation of the background with equivalence ratio might reflect the variation of flame temperature, since CO_2 and H_2O absorption is strongly temperature dependent.[19,21]

The interference from the broadband background signal is not negligible in these flames and can become a problem in practical applications.

G. Temperature Sensitivity

Quantitative NO concentration measurements without the exact knowledge of local temperature require choosing a transition that minimizes the temperature sensitivity. The main temperature influence of NO LIF signal strength arises from the ground-state population of the laser-coupled levels. Since line broadening and shifting is temperature dependent,
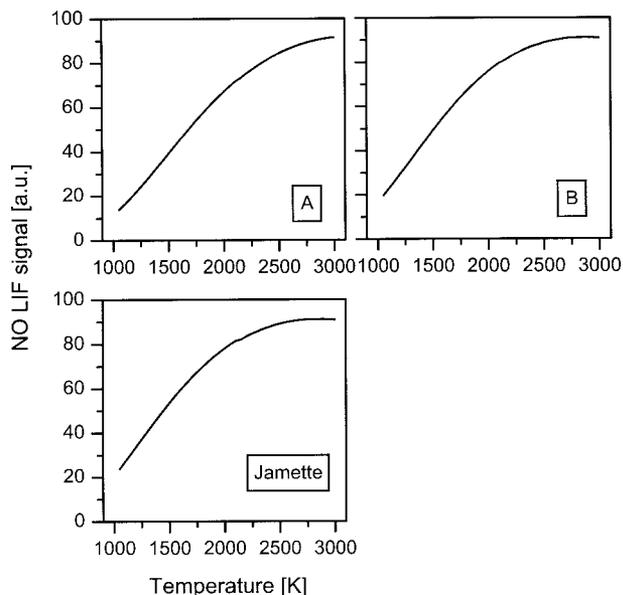
Fig. 14. Temperature dependence of the NO LIF signal when number density is evaluated. Simulation for $p = 10$ bar.

Fig. 15. Temperature dependence of the NO LIF signal when mole fraction is evaluated. Simulation for $p = 10$ bar.

the overlap of the spectral features with the spectral shape of the laser also shows temperature dependence. Temperature furthermore influences the fluorescence quantum yield by changing collisional frequencies and quenching cross sections. This influence is identical for all transitions, since the quenching rates do not vary with rotational state for NO. Nevertheless, the resulting temperature dependence was included in the calculations with the Paul models for quenching-rate coefficients,[36,37] assuming equilibrium exhaust gas concentrations of a $\phi = 0.9$ flame.

The combined temperature effects of ground-state population, spectral overlap, and quantum yield were calculated for the 10-bar flame and a 0.4-cm^{-1} laser FWHM based on a nontransient four-level LIF model.[14] Figure 14 shows the temperature sensitivity of LIF intensities for constant NO number densities. Because of the high ground-state energies of $A–X(0,1)$ transitions [the vibrational energy of the $X(v'' = 1)$ state is 1876 cm^{-1} (Ref. 38)], maximum LIF signal corresponding to maximum population is found at high temperatures of >2800 K for all three transitions, and signals are strongly decreasing toward lower temperatures. Correction for this temperature effect is necessary for interpretation of the LIF signal when NO number densities are measured.

In many combustion situations not only the measurement of local NO number density but also the direct measurement of mole fractions $x_{NO} = N_{NO}/N_{total}$ is necessary. Because of the $1/T$ dependence of N_{total}, the resulting temperature dependencies of LIF intensities are altered. Typically this reduces the temperature sensitivity of hot transitions in the moderate temperature range and thus enables their use for quantitative measurements without temperature corrections.[8,14,28] The results of this approach
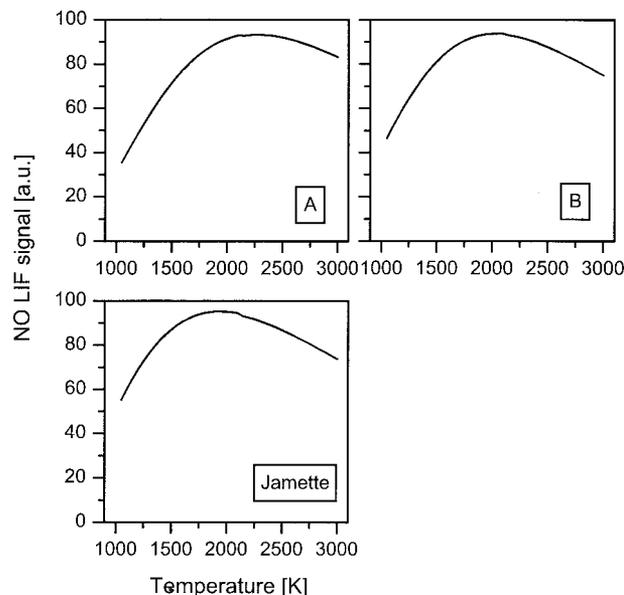
are shown in Fig. 15. Maximum NO LIF signal is found at temperatures of 2300, 2050, and 1950 K for the A, B, and Jamette transitions, respectively, and the variation of the signal between 1500 and 3000 K is ±12, 11, and 12%, respectively. This corresponds to the systematic error that is induced in NO concentration measurements when no temperature information is available for correction of the LIF signals. The error is approximately equal for all transitions, depending on the specific range of temperatures that are present in the investigated system.

5. Summary

Laser-induced fluorescence measurements were performed for NO $A–X(0,1)$ excitation in laminar, premixed methane/air flames between 1 and 60 bar with equivalence ratios between 0.83 and 1.13. Three different excitation strategies were chosen in the (0,1) band as most promising candidates. They were compared for feasibility of selective and quantitative NO diagnostics in high-pressure flames.

Of the three strategies, the $R_1 + Q_{21}(22.5)$, $Q_1 + P_{21}(8.5)$, $Q_2 + R_{12}(17.5)$ (Jamette) excitation feature at 236.22 nm shows strongest NO LIF signals and best independence of pressure-shifting effects, making it the candidate of choice in the absence of O_2 (e.g., rich flames). In lean flames, however, the transition experiences a high interference of O_2 LIF (33–36% for red-shifted detection in the 60-bar $\phi = 0.83$ flame). This interference can be significantly reduced to 15–18% by use of the $P_1(25.5)$, $R_1 + Q_{21}(11.5)$, $Q_1 + P_{21}(17.5)$ (B) feature at 235.87 nm. The $R_1 + Q_{21}(16.5)$, $P_2 + Q_{12}(32.5)$, $P_{21}(22.5)$, $O_{12}(40.5)$ (A) feature at 235.55 nm has no particular advantage in signal strength or interference. Fine tuning the laser to maximum NO/O_2 ratio for each individual

pressure is advantageous for both maximizing signal strength and minimizing interference.

A broadband background signal is present independently of excitation wavelength, only slightly dependent on equivalence ratio, and with an intensity that increases approximately linearly with pressure. The origin of this signal is not yet clear. The signal causes additional interference with red-shifted detection independent of the air/fuel ratio.

References

1. A. C. Eckbreth, *Laser Diagnostics for Combustion, Temperature, and Species*, 2nd ed. (Gordon and Breach, Amsterdam, The Netherlands, 1996).

2. K. Kohse-Höinghaus, "Laser techniques for the quantitative detection of reactive intermediates in combustion systems," Prog. Energy Combust. Sci. **20,** 203–279 (1994).

3. K. Kohse-Höinghaus and J. B. Jeffries, *Applied Combustion Diagnostics* (Taylor and Francis, New York, 2002).

4. T. M. Brugmann, G. G. M. Stoffels, N. Dam, W. L. Meerts, and J. J. ter Meulen, "Imaging and post-processing of laser-induced fluorescence from NO in a Diesel engine," Appl. Phys. B **64,** 717–724 (1997).

5. C. S. Cooper and N. M. Laurendeau, "Parametric study of NO production via quantitative laser-induced fluorescence in high-pressure, swirl-stabilized spray flames," in *Proceedings of the Combustion Institute* (Combustion Institute, Pittsburgh, Pa., 2002), Vol. 28, pp. 287–293.

6. J. E. Dec and R. E. Canaan, "PLIF imaging of NO formation in a DI Diesel engine," SAE 980147 (Society of Automotive Engineers, Warrendale, Pa., 1998).

7. A. Bräumer, V. Sick, J. Wolfrum, V. Drewes, R. R. Maly, and M. Zahn, "Quantitative two-dimensional measurements of nitric oxide and temperature distributions in a transparent SI engine," SAE 952462 (Society of Automotive Engineers, Warrendale, Pa., 1995).

8. W. G. Bessler, C. Schulz, M. Hartmann, and M. Schenk, "Quantitative in-cylinder NO-LIF imaging in a direct-injected gasoline engine with exhaust gas recirculation," SAE 2001-01-1978 (Society of Automotive Engineers, Warrendale, Pa., 2001).

9. F. Hildenbrand, C. Schulz, J. Wolfrum, F. Keller, and E. Wagner, "Laser diagnostic analysis of NO formation in a direct injection Diesel engine with pump-line nozzle and common-rail injection systems," in *Proceedings of the Combustion Institute* (Combustion Institute, Pittsburgh, Pa., 2000), Vol. 28, pp. 1137–1144.

10. J. M. Seitzman, G. Kychakoff, and R. K. Hanson, "Instantaneous temperature field measurements using planar laser-induced fluorescence," Opt. Lett. **10,** 439–441 (1985).

11. B. K. McMillin, J. L. Palmer, and R. K. Hanson, "Temporally resolved, two-line fluorescence imaging of NO temperature in a transverse jet in a supersonic cross flow," Appl. Opt. **32,** 7532–7545 (1993).

12. W. G. Bessler, F. Hildenbrand, and C. Schulz, "Two-line laser-induced fluorescence imaging of vibrational temperatures of seeded NO," Appl. Opt. **40,** 748–756 (2000).

13. J. L. Palmer and R. K. Hanson, "Shock tunnel flow visualization using planar laser-induced fluorescence imaging of NO and OH," Shock Waves **4,** 313–323 (1995).

14. W. G. Bessler, C. Schulz, T. Lee, D.-I. Shin, J. B. Jeffries, and R. K. Hanson, "Strategies for laser-induced fluorescence detection of nitric oxide in high-pressure flames. I. A–X(0,0) excitation," Appl. Opt. **41,** 3547–3557 (2002).

15. W. G. Bessler, C. Schulz, T. Lee, J. B. Jeffries, R. K. Hanson, continuing in their series, are preparing a manuscript to be called "Strategies for laser-induced fluorescence detection of nitric oxide in high-pressure flames. III. Comparison of A–X excitation schemes."

16. T. Lee, D.-I. Shin, J. B. Jeffries, R. K. Hanson, W. G. Bessler, and C. Schulz, "Laser-induced fluorescence detection of NO in high-pressure flames with A–X(0,0), (0,1), and (0,2) excitation," presented at the 40th Aerospace Sciences Meeting, Reno, Nev. 14–17 January 2002, paper AIAA-2002-0399.

17. W. G. Bessler, C. Schulz, T. Lee, J. B. Jeffries, and R. K. Hanson, "Laser-induced-fluorescence detection of nitric oxide in high-pressure flames with A–X(0,1) excitation," presented at the Western States Section/The Combustion Institute, 2001 Spring Meeting, Oakland, Calif.

18. F. Hildenbrand and C. Schulz, "Measurements and simulation of in-cylinder UV-absorption in spark ignition and Diesel engines," Appl. Phys. B **73,** 165–172 (2001).

19. C. Schulz, J. D. Koch, D. F. Davidson, J. B. Jeffries, and R. K. Hanson, "Measurements of ultraviolet absorption spectra of shock heated carbon dioxide and water between 900 and 2800 K," Chem. Phys. Lett. **355,** 82–88 (2002).

20. W. G. Bessler, C. Schulz, T. Lee, D.-I. Shin, M. Hofmann, J. B. Jeffries, J. Wolfrum, and R. K. Hanson, "Quantitative NO-LIF imaging in high-pressure flames," Appl. Phys. B **75,** 97–102 (2002).

21. C. Schulz, J. B. Jeffries, D. F. Davidson, J. D. Koch, J. Wolfrum, and R. K. Hanson, "Impact of UV absorption by CO_2 and H_2O on NO LIF in high-pressure combustion applications," Proc. Combust. Inst. (to be published).

22. G. Herzberg, *Molecular Spectra and Molecular Structure, Vol. I: Spectra of Diatomic Molecules* (Krieger, Malabar, Fla., 1950).

23. M. D. DiRosa and R. K. Hanson, "Collision-broadening and -shift of NO γ(0,0) absorption lines by H_2O, O_2 and NO at 295 K," J. Mol. Spectrosc. **164,** 97–117 (1994).

24. M. D. DiRosa and R. K. Hanson, "Collisional broadening and shift of NO γ(0,0) absorption lines by O_2 and H_2O at high temperatures," J. Quant. Spectrosc. Radiat. Transfer **52,** 515–529 (1994).

25. A. O. Vyrodov, J. Heinze, and U. E. Meier, "Collisional broadening of spectral lines in the A–X(0,0) system of NO by N_2, Ar, and He at elevated pressures measured by laser-induced fluorescence," J. Quant. Spectrosc. Radiat. Transfer **53,** 277–287 (1995).

26. F. Hildenbrand, C. Schulz, V. Sick, H. Jander, and H. Gg. Wagner, "Applicability of KrF excimer laser induced fluorescence in sooting high-pressure flames," VDI Flammentag Dresden, VDI Berichte 1492 (ISBN 3-18-091492-0), 269–274 (1999).

27. C. Schulz, V. Sick, J. Wolfrum, V. Drewes, M. Zahn, and R. Maly, "Quantitative 2D single-shot imaging of NO concentrations and temperatures in a transparent SI engine," in *Proceedings of the Combustion Institute* (Combustion Institute, Pittsburgh, Pa., 1996), Vol. 26, pp. 2597–2601).

28. F. Hildenbrand, C. Schulz, F. Keller, G. König, and E. Wagner, "Quantitative laser diagnostic studies of the NO distribution in a DI Diesel engine with PLN and CR injection systems," SAE

2001-01-3500 (Society of Automotive Engineers, Warrendale, Pa., 2001).

29. P. Jamette, P. Desgroux, V. Ricordeau, and B. Deschamps, "Laser-induced fluorescence detection of NO in the combustion chamber of an optical GDI engine with $A–X(0,1)$ excitation," SAE 2001-01-1926 (Society of Automotive Engineers, Warrendale, Pa., 2001).

30. M.-S. Chou, A. M. Dean, and D. Stern, "Laser induced fluorescence and absorption measurements of NO in NH_3/O_2 and CH_4/air flames," J. Chem. Phys. **78,** 5962–5970 (1983).

31. P. A. Berg, G. P. Smith, J. B. Jeffries, and D. R. Crosley, "Nitric oxide formation and reburn in low-pressure methane flames," in *Proceedings of the Combustion Institute* (Combustion Institute, Pittsburgh, Pa., 1998), Vol. 27, pp. 1377–1384.

32. L. Pillier, C. Moreau, X. Mercier, J. F. Pauwels, and P. Desgroux, "Quantification of stable minor species in confined flames by cavity ring-down spectroscopy: application to NO," Appl. Phys. B **74,** 427–434 (2002).

33. H. Eberius, T. Just, T. Kick, G. Höfner, and W. Lutz, "Stabilization of premixed, laminar methane flames in the pressure regime up to 40 bar," in *Proceedings of the Joint Meeting German/Italian Section of the Combustion Institute* (Combustion Institute, Pittsburgh, Pa., 1989), paper 3.3.

34. C. Schulz, V. Sick, U. Meier, J. Heinze, and W. Stricker, "Quantification of NO $A–X(0,2)$ LIF: investigation of calibration and collisional influences in high-pressure flames," Appl. Opt. **38,** 1434–1443 (1999).

35. L. G. Piper and L. M. Cowles, "Einstein coefficients and transition moment variation for the NO ($A^2\Sigma^+ - X^2\Pi$) transition," J. Chem. Phys. **85,** 2419–2422 (1986).

36. P. H. Paul, J. A. Gray, J. L. Durant Jr., and J. W. Thoman Jr., "A model for temperature-dependent collisional quenching of NO $A^2\Sigma^+$," Appl. Phys. B **57,** 249–259 (1993).

37. P. H. Paul, C. D. Carter, J. A. Gray, J. L. Durant Jr., J. W. Thoman, and M. R. Furlanetto, "Correlations for the NO $A^2\Sigma^+$ ($v' = 0$) electronic quencing cross-section," Sandia Rep. SAND94–8237 UC-1423 (Sandia National Laboratory, Livermore, Calif., 1995).

38. P. H. Paul, "Calculation of transition frequencies and rotational line strengths in the γ-bands of nitric oxide," J. Quant. Spectrosc. Radiat. Transfer **57,** 581–589 (1997).